Cleaner Engineering and Technology 29 (2025) 101090

Contents lists available at ScienceDirect

Cleaner Engineering and Technology

journal homepage: www.sciencedirect.com/journal/cleaner-engineering-and-technology

Recycled aggregate concrete confined with FRP under compression: A machine learning-driven framework and parametric analysis

Hossein Saberi [a,*], Hamid Saberi [b]

[a] Hamburg University of Technology, TUHH, Numerical Structural Analysis with Application in Ship Technology (M-10), Am Schwarzenberg-Campus 4 (C), 21073 Hamburg, Germany
[b] Department of Petroleum and Natural Gas Engineering, Sahand University of Technology, Tabriz, Iran

ARTICLE INFO

Keywords:
Machine learning
Recycled aggregate concrete
FRP-confined
Stress-strain relationships
SVD decomposition

ABSTRACT

Modeling the compressive behavior of fiber-reinforced polymer (FRP)-confined recycled aggregate concrete (RAC) is essential for practical engineering applications. Existing models often overlook the nonlinear effects of recycled aggregate content on concrete strength, limiting their accuracy. To address this gap and promote sustainable construction, this study proposes a novel approach for predicting the stress-strain behavior of FRP-confined RAC under compression. The method integrates clustering techniques and singular value decomposition (SVD) to extract nonlinear relationships between key system parameters and stress-strain curves. The least squares method is then used to optimize unknown system parameters. A dataset comprising 81 stress-strain curves from eight references, totaling 2452 digitized data points at a strain rate of 0.0005, was used to train the model. The proposed approach is validated against experimental results, demonstrating high accuracy in capturing the mechanical behavior of FRP-confined RAC. These findings provide a more reliable predictive tool for structural engineers and contribute to the advancement of sustainable concrete technologies.

Nomenclature	
E_1	Initial elastic modulus of FRP-confined concrete
E_2	Slope of the asymptotic line in the hardening phase of the curve
E_c	Concrete elastic modulus
E_{frp}	FRP Elastic modulus
R	Replacement percentage
D	Specimen diameter
f_{cc}	FRP-confined concrete ultimate strength
f_{frp}	FRP ultimate tensile strength
f_0	Stress at the intersection of the back-extended asymptotic line
f_{co}	Unconfined concrete compressive strength
n	Curve shape parameter
ε_{c0}	Axial peak strain
ε_{cu}	Ultimate strain of FRP-confined concrete
ε_{frp}	FRP ultimate strain
t_{frp}	FRP thickness
k_ε	Strain efficiency factor of FRP
$A_{r\times r}$	Norm matrix
h	Coefficient of fuzzification
$\mu = \left\{\vec{\mu}_1, \ldots, \vec{\mu}_c\right\}$	Cluster centers

(*continued on next column*)

(*continued*)

Nomenclature	
u_{ij}	Belongness of j^{th} data to the i^{th} cluster
Φ	Basis vector
τ	Membership degree

1. Introduction

With the increasing population and the push for urbanization, numerous structures currently need extensive repairs or may require replacement. This situation arises because these structures have either reached or are approaching the end of their service life, were not built to the required specifications, or have not been properly maintained throughout their use. Additionally, even structures that have not yet completed their intended lifespan may need to be taken down to adhere to updated zoning laws and contemporary urban planning standards (Chen et al., 2019). These repair and replacement processes produce significant quantities of waste concrete that need to be disposed of properly (Ho et al., 2021).

Data gathered from several countries across 6 continents indicates

* Corresponding author.
E-mail address: hossein.saberi@tuhh.de (H. Saberi).

https://doi.org/10.1016/j.clet.2025.101090
Received 10 June 2025; Received in revised form 18 September 2025; Accepted 4 October 2025
Available online 10 October 2025

that the total generation of demolition and construction waste surpassed 3 billion tons for a year by 2012, and this trend is on the rise (Akhtar et al., 2018). In 2020, Japan generated approximately 78.21 million tons of demolition and construction waste (Zhao et al., 2023). Concrete debris is often sent to distant landfills, resulting in transportation expenses, heightened greenhouse gas emissions, the consumption of valuable landfill space, and contributing to environmental pollution (Chen et al., 2016a).

The buildup of construction and demolition waste poses significant environmental challenges. Firstly, the accumulation of urban construction waste occupies significant land, alters the physical, chemical properties and composition of the soil, degrades soil structure, and reduces fertility. Secondly, during the accumulation process, construction waste releases harmful gases and odors. Bacteria, dust, and lightweight debris from the waste can be blown into the atmosphere, contributing to air pollution. Thirdly, as waste is piled and landfilled, it generates leachate containing a variety of metal and non-metal pollutants, which can severely contaminate surface and groundwater sources. Finally, when construction waste is haphazardly piled and not cleared promptly, it consumes vast urban space (Chen et al., 2019).

To mitigate the negative impacts of handling deconstruction waste, it is worth investigating the utilization of this demolished concrete as aggregate in concrete. Recycled Aggregate Concrete (RAC) has been considered as a sustainable and eco-friendly construction material, attracting the interest of many studies (Fathifazl et al., 2011; Topçu et al., 2008; Gholampour et al., 2018; Ozbakkaloglu et al., 2018; Chen et al., 2014; Kang et al., 2014). In this type of concrete, natural aggregates are either partially or fully substituted with recycled aggregates, which are created by grading, washing, and crushing waste concrete. The benefits of recycling aggregates include: (i) the chance to repurpose a widely used construction material, (ii) reducing environmental pollution, (iii) conserving valuable landfill space, and (iv) conserving natural resources (Xu et al., 2017a, 2017b; Chen et al., 2016b; Wu et al., 2013).

Despite these environmental benefits, RAC exhibits the properties that differ related to the natural aggregates, which may limit its widespread use. Research has shown that old mortar adhered to the surface of RCA leads to increased water absorption and higher porosity (Padmini et al., 2009; Corinaldesi, 2010; Tam et al., 2005; Ferreira et al., 2011; Silva et al., 2015). Additionally, the crushing process of RCA forms cracks that can reduce compressive strength in comparison to the natural aggregates (Olorunsogo et al., 2002; Nagataki et al., 2004; Xiao et al., 2012; Pedro et al., 2015).

It has been widely demonstrated that FRP confinement significantly enhances the compressive strength and ductility of concrete, particularly for materials with inherently brittle behavior such as ultra-high performance concrete (UHPC). Numerous studies have explored the key parameters influencing the behavior of FRP-confined concrete, including the effects of fiber type, confinement ratio, and specimen geometry. For instance, recent investigations on FRP-confined UHPC have highlighted the positive effects of steel fibers, FRP thickness, and confinement uniformity on improving both strength and ductility, while also identifying the limitations of existing models in capturing post-peak behavior (Liao et al., 2021). Additionally, new design-oriented models have been proposed to describe the axial stress–strain response of FRP-confined UHPC, accommodating both typical bilinear behavior and cases where stress reduction-recovery phenomena occur (Liao et al., 2022). These findings align with broader research showing that FRP-confined concrete can exhibit complex three-stage behavior (hardening-softening-rehardening) under axial compression, governed by factors such as brittleness, shrinkage, and non-uniform confinement (Liao et al., 2023).

Zhao et al. (2015) presented the findings from 18 axial compression tests on FRP-confined RAC. Key conclusions include: i) RAC with a 20 % replacement ratio performs similarly to natural aggregate concrete (NAC), both with and without FRP confinement; ii) Teng et al.'s model (Teng et al., 2009) and Jiang and Teng's model (Jiang et al., 2007) are accurate for prediction of the ultimate axial stress and tend to overestimate the ultimate strain, particularly for FRP-confined RAC; and iii) notable discrepancies exist between the test results and the predictions of these two stress-strain models. Chen et al. (2016a) presented the results of numerous compression tests on CFRP-confined RAC cylinders, focusing on two key test parameters: the coarse aggregate replacement ratio and the stiffness of the CFRP jacket. Chen et al. (2018) reported axial compression tests on FRP-confined NAC and RAC specimens in 3 scales, diameters change between 150 mm and 300 mm. Specimens of varying sizes were designed with identical FRP confinement stiffness to investigate potential size effects in FRP-confined RAC for the first time. The results show no significant size effect in either FRP-confined NAC or RAC within the tested size range. Additionally, the effectiveness of FRP confinement was found to be only slightly impacted by the recycled aggregates. Wang et al. (2024) proposed a model for FRP-confined RAC under compression load by using the confining stress path. The model introduces an effect index to represent the effect of the confining stress path on the concrete compressive strength. Relationships between the confinement ratio and the effect index, as well as between the confinement ratio and the lateral stress index, are established. Validation of the model through comparing result of it with prior experimental results and previous models shows that the FRP-confined RAC compressive strength is influenced by the confinement path at low ratios (below 0.43) but it is independent at higher ratios (above 0.43).

Several studies have utilized machine learning (ML) techniques and artificial intelligence (AI) methods to predict the compressive strength (CS) of FRP-confined concrete cylinders, addressing the challenges associated with the complexity and variability of concrete behavior under confinement. Cevik and Guzelbey (Cevik et al., 2008) applied a neural network (NN) model to predict the confined CS of CFRP-wrapped cylinders. They used 101 data points from seven different studies, incorporating input parameters like the cylinder's diameter, unconfined CS, FRP tensile strength, and FRP thickness. The NN model's results demonstrated high accuracy with an R-value of 0.98 when compared to experimental data. Their approach outperformed existing models in terms of prediction accuracy. Elsanadedy et al. (2012) predicted the CS and strain of FRP-confined cylinders using both regression and ANN models. They trained a single hidden-layer NN and found that the ANN model provided more accurate predictions compared to existing mathematical relationships. Jalal and Ramezanianpour (Jalal et al., 2012) also employed ANN to enhance the prediction of the CS of FRP-confined concrete cylinders. By using a dataset of 128 specimens, their model showed a mean error of around 10 %, demonstrating better accuracy compared to five existing models. Pham and Hadi (Pham et al., 2014) applied ANN to predict the CS and strain of FRP-confined square and rectangular columns, using 104 datasets for rectangular columns and 69 for square columns. Their model achieved high accuracy, with the correlation factor reaching 96 % for rectangular columns and 98 % for square columns. Their results indicated the potential of ANN in predicting the behavior of FRP-confined concrete columns with different cross-sectional shapes. Moreover, Kamgar et al. (2020) investigated the ultimate FRP-confined CS of cylinders using the feed-forward back-propagation neural network (FFBPNN). They proposed a new model that achieved an R-value of 0.9809 and a low error percentage of 3.49 %. Their results were more accurate and precise compared to existing models. Keshtegar et al. (2021)combined support vector regression (SVR) and response surface modeling (RSM) to predict the CS of FRP-confined cylinders. Their hybrid model showed robust behavior with low mean absolute error (MAE) and root mean square error (RMSE) values, outperforming other models. Kumar et al. (2022)used various machine learning models, including GPR, SVM, and ensemble learning (EL), to predict the CS of lightweight concrete (LWC). They optimized these models and found that the optimized GPR model outperformed others with an R-value of 0.9803. Their study also highlighted the efficiency of SVMR and EL models. In another study, Kumar et al. (2023)

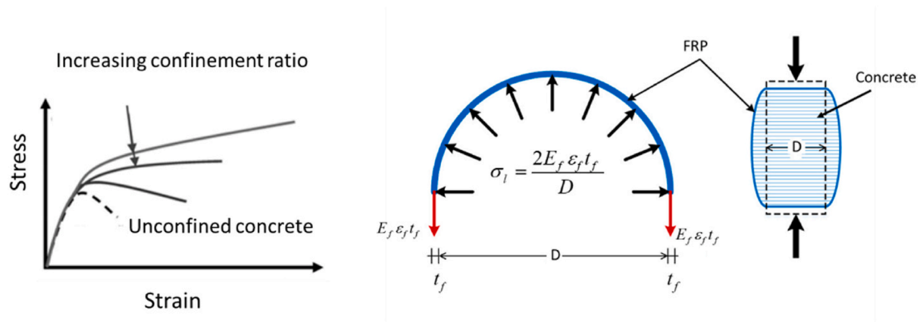

Fig. 1. The effect of confinement on the compressive behavior of concrete.

evaluated the CS of fly-ash-based geopolymer concrete using optimized SVM, GPR, and EL models, achieving an R-value of 0.9590 with the optimized GPR model, outperforming other models in terms of accuracy. Jamali et al. (2022) used machine learning models, such as multi-layer perceptron (MLP), SVR, and a combination of ANFIS with particle swarm optimization (PSO), to predict the CS. Their study also employed the Kriging interpolation method for CS prediction. Among the models tested, the Kriging method showed the highest accuracy with an R-value of 0.985, outperforming the SVR and MLP models. In conclusion, these studies demonstrate the effectiveness of machine learning techniques, particularly ANN, genetic programming, and support vector regression, in accurately predicting the CS of FRP-confined concrete cylinders. These models not only offer higher accuracy compared to traditional methods but also provide valuable tools for optimizing concrete designs in construction engineering. Duan et al. (2013a) implemented an ANN using 168 data sets, highlighting its effectiveness for this purpose. Similarly, Younis and Pilakoutas (Younis et al., 2013) applied multiple linear regression (MLR) and nonlinear regression analysis for CS estimation, while also highlighting the positive impact of incorporating steel fibers from recycled tires into RAC. Khademi et al. (2016a) assessed the predictive capabilities of AI techniques, including ANN, ANFIS, and MLR, in estimating CS. Their findings indicated that ANN demonstrated the highest accuracy, with an R^2 value of 0.919 and a mean squared error (MSE) of 19.768. However, ANFIS posed challenges related to weight assignment in the membership function, necessitating the application of optimization or metaheuristic algorithms to refine its accuracy (Khosravi et al., 2018a, 2018b). Beyond ANN and ANFIS, other AI-based approaches, such as support vector machines (SVM) and extreme learning machines (ELM), have also been employed. These methods, however, come with challenges such as high computational demands for large datasets, slow learning rates, and scalability issues (Zhang et al., 2005, 2008; Huang et al., 2011). In a separate study, Abdollahzadeh et al. (2016) explored gene expression programming (GEP) as a predictive tool for CS, particularly for RAC incorporating silica fume. While their results were promising, their study did not incorporate optimization techniques or comparative analyses with benchmark models. Deep learning methods, such as convolutional neural networks (CNNs), have also been explored for CS prediction. Deng et al. (2018) examined the use of CNNs on 74 concrete block samples, concluding that CNNs offered superior generalization ability, efficiency, and precision compared to conventional techniques. Further research on AI-based CS prediction models can be found in (Dantas et al., 2013; Omran et al., 2016; Khademi et al., 2016b; Naderpour et al., 2018), with an extensive review of related methodologies available in (Asteris et al., 2019a, 2019b; Liu et al., 2020).

Although sustainable construction materials have gained increasing attention, there is still a notable lack of research on the behavior of RAC under confined conditions. While several studies have examined the mechanical properties of RAC without confinement, its behavior when confined has not been sufficiently explored. This is particularly important given the growing application of recycled aggregates in structural elements subjected to high confinement, such as columns and shear walls. Confined concrete behavior plays a crucial role in determining the material's strength, ductility, and failure patterns, making accurate modeling essential for safe structural design. To advance the use of RAC in structural engineering and enhance sustainability in construction, further investigation is necessary to develop more reliable models, particularly for predicting stress-strain curves, which is the primary motivation for this study. The key innovations of this contribution is summarized as follows.

- A new method for modeling the behavior of FRP-confined RAC is offered.
- • The structure of the proposed model is such that it facilitates the use of the least squares method to optimize the model parameters.
- The SVD decomposition is utilized to calculate the basis vectors of the experimental stress-strain curves, which are incorporated into the structure of the proposed method.
- 81 experimental curves from 8 previous studies was extracted that is used for training the proposed method's parameters.
- A comparison is made between the results of the proposed method and those obtained from experiments and other previous models.
- A simple empirical stress-strain model is proposed.

The remaining of this study is organized as follows.

Section 2 highlights the significance of the research conducted in this study. Section 3 introduces a novel ML-driven framework for modeling the behavior of FRP-confined RAC under compressive load. Section 4 provides detailed test results and an assessment of the proposed method. Section 5 reports the results and discusses them. Section 6 is dedicated to presenting a simple empirical stress-strain model. Section 7 addresses limitations and outlines future work. Finally, Section 8 provides a summary of the findings.

2. Research significant

It is well known that applying lateral confinement to concrete significantly improves its strength and ductility. With the advent of FRP-composites in the construction industry, their use as a confinement material has gained considerable attention. Over the past two decades, numerous experimental and analytical studies have been carried out to investigate and model the compressive behavior of FRP-confined concrete. In circular concrete sections confined with FRP, the lateral confining pressure (σ_l) exerted by the FRP shell can be considered uniformly distributed around the circumference (Fig. 1). This confinement mechanism is passive, meaning the pressure develops in response to the lateral expansion of concrete under axial compression. As the FRP shell undergoes tensile stress in the hoop direction, the confining pressure (σ_l) increases in proportion to this expansion until the system ultimately fails due to the rupture of the FRP shell. As shown in Fig. 1, as the lateral confining pressure increases, the specimen is able to withstand higher compressive forces, causing the stress-strain curve to shift toward higher

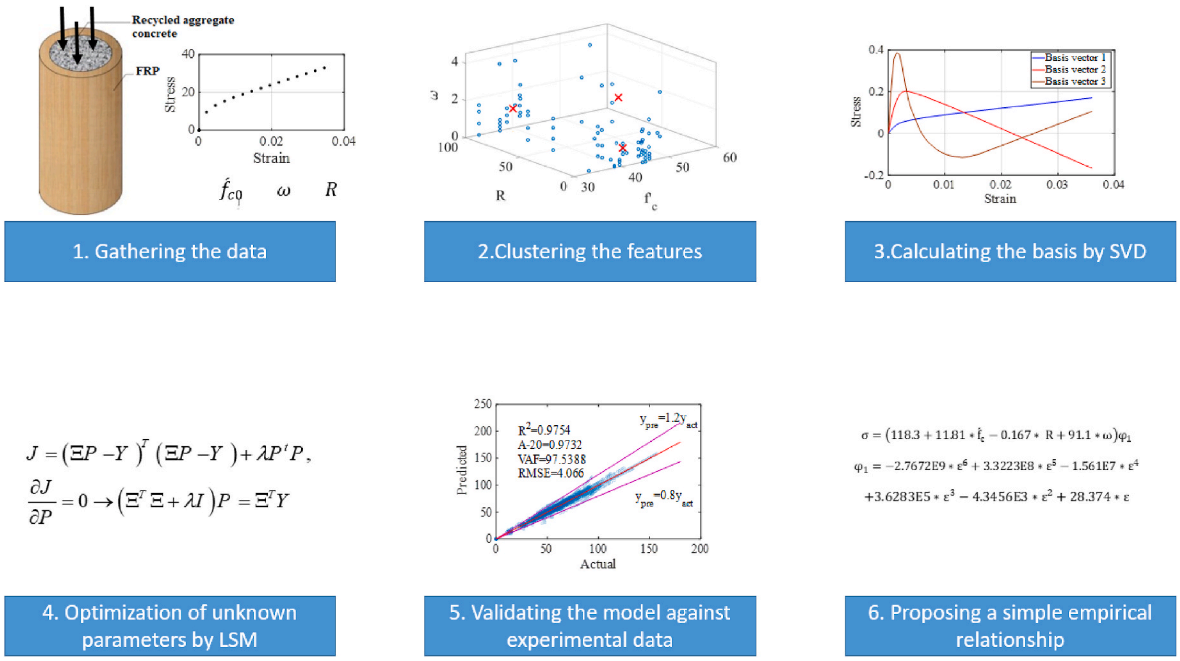

Fig. 2. Graphical abstract of this study.

values.

The growing emphasis on sustainable construction practices has led to an increased interest in the application of RAC. As a viable alternative to conventional concrete, RAC not only helps reduce waste but also minimizes the environmental impact of extracting and processing natural aggregate (Chen et al., 2019; Ho et al., 2021). Despite its potential benefits, the mechanical behavior of RAC, particularly when subjected to confinement under compressive loads, remains poorly understood. This gap in knowledge poses significant challenges for practical applications, as existing modeling techniques often do not adequately capture the unique properties of RAC.

The primary concern lies in the inherent variability of recycled aggregates, which are derived from demolished concrete structures. These aggregates can exhibit differences in shape, size, composition, etc., which can lead to unpredictable mechanical behavior. In the existing body of research on confined recycled aggregate concrete (RAC), a significant limitation is the reliance on a narrow set of experimental data, often derived from limited studies by a single researcher or group. Many of the available models for predicting the behavior of confined RAC under compression have been developed based on experimental data that do not account for the diversity of RAC compositions or environmental factors (Chen et al., 2016a) (Zhou et al., 2016) (Chen et al., 2018) (Zhao et al., 2015). As a result, these models may fail to capture the full range of mechanical behaviors that may arise when using recycled aggregates from different sources or with varying characteristics. Thus, there is an urgent need for a comprehensive approach that not only considers experimental data from a wider range of studies but also develops models that precisely reflect the behavior of FRP-confined RAC.

In recent years, the application of artificial intelligence methods in modeling the behavior of recycled materials has gained significant attention (Armaghani et al., 2024; Asteris et al., 2024; Hosseini et al., 2024; Rezaei et al., 2024; Saberi et al., 2022; Fattahi et al., 2024). Techniques such as neural networks and fuzzy systems have been utilized to predict properties like compressive strength (Topçu et al., 2008; Duan et al., 2013a, 2021; Khademi et al., 2016a; Deng et al., 2018; Dantas et al., 2013), tensile strength (Topçu et al., 2008; Xu et al., 2019), and modulus of elasticity of concrete (Xu et al., 2019; Duan et al., 2013b).

The application of ML-based methods in predicting the behavior of FRP-confined recycled aggregate concrete (RAC) under compression is still quite limited. Most existing machine learning approaches in this domain have primarily focused on predicting specific parameters, such as peak stress or strain, rather than capturing the complete stress-strain response. However, none of these methods have been applied to the prediction of stress-strain curves of RAC. This study presents a novel approach by focusing on stress-strain curve prediction of FRP-confined concrete containing recycled aggregates under compressive loading for the first time. The graphical abstract of this study is illustrated in Fig. 2.

3. Methodology

Fuzzy systems, particularly the Mamdani and Sugeno models, are well-known in the field of fuzzy logic for their effectiveness in handling complex decision-making, control systems, and pattern recognition tasks. A newer fuzzy system, introduced by the author in 2017 (Saberi et al., 2017), is based on the clustering of the input data and serves as the basis for the method proposed in this study. Similar to the Sugeno system, this approach generates crisp outputs directly from its rules. However, unlike both the Mamdani and Sugeno systems, the membership functions in this method are defined based on clusters across multiple dimensions, depending on the problem's complexity. This design allows for the direct calculation of membership degrees to combine rules, eliminating the need for T-norm or S-norm operations. As a result, the system's unknown parameters can be optimized more easily, efficiently, and stably using the least squares method. In this study, since the primary focus is predicting stress-strain curves, the output of each rule consists of basis curves, which are derived from the singular value decomposition (SVD) of existing FRP-confined RAC curves. The mathematical details of the proposed method are outlined as follows.

The purpose of clustering approaches, for instance Fuzzy C-means (FCM), is to partition a dataset $X = \left\{ \vec{x}^{1}_{1\times r}, \ldots, \vec{x}^{N}_{1\times r} \right\} \subset \mathbb{R}^r$ into subgroups based on feature similarity. This similarity is measured through the distance between cluster centers and data points. A shorter distance indicates greater similarity. Consequently, the FCM algorithm seeks to minimize a cost function, which represents the sum of the weighted

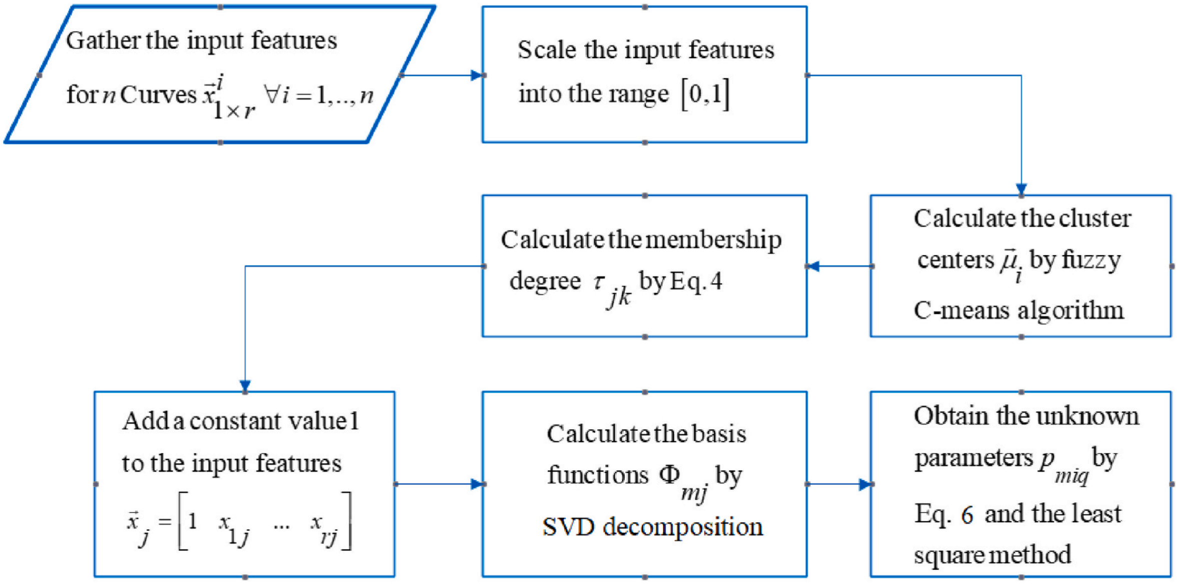

Fig. 3. The flowchart of the proposed model.

distances between cluster centers and their corresponding data points, defined as:

$$J(U,\mu;X)=\sum_{j=1}^{N}\sum_{i=1}^{c}u_{ij}^{h}\left\|\vec{x}_j-\vec{\mu}_i\right\|_A^2,\ \sum_{i=1}^{c}u_{ij}=1,u_{ij}>0, \tag{1}$$

The distance, denoted as $\left\|\vec{x}_j-\vec{\mu}_i\right\|_A^2=\left(\vec{x}_j-\vec{\mu}_i\right)^T A\left(\vec{x}_j-\vec{\mu}_i\right)$, and the norm matrix as $A_{r\times r}$. The term $h>1$ represents the coefficient of fuzzification, and the number of clusters is determined by c. The weights u_{ij} indicate the degree to which the j^{th} data belongs to the i^{th} fuzzy cluster. These weights and the centers $\mu=\left\{\vec{\mu}_1,\dots,\vec{\mu}_c\right\}$, are computed iteratively using the following procedure (Askari et al., 2017):

$$\vec{\mu}_i=\frac{\sum_{j=1}^{N}u_{ij}^{h}\,\vec{x}_j}{\sum_{j=1}^{N}u_{ij}^{h}},\ u_{ij}=\left[\sum_{k=1}^{c}\left(\frac{\left\|\vec{x}_j-\vec{\mu}_i\right\|_A^2}{\left\|\vec{x}_j-\vec{\mu}_k\right\|_A^2}\right)^{\frac{1}{h-1}}\right]^{-1}. \tag{2}$$

A combination of the above-mentioned FCM and SVD decomposition of experimental stress-strain curves, serves as a basis function for each rule output, is applied to model the behavior of FRP-confined RAC.

Consider n input curves with r features $X=\left\{\vec{x}^{1}_{1\times r},\dots,\vec{x}^{n}_{1\times r}\right\}$ and their corresponding data $\left\{\left(\vec{z}^{1}_{1\times t_1},\vec{y}^{1}_{1\times t_1}\right),\dots,\left(\vec{z}^{n}_{1\times t_n},\vec{y}^{n}_{1\times t_n}\right)\right\}$, where t_λ denotes the number of data at the λ^{th} curve. The approximation j^{th} curve can be expressed as:

$$Output_j=\sum_{m=0}^{w}\Phi_{mj}\times\sum_{i=1}^{c}\tau_{ji}\times\sum_{q=0}^{r}p_{miq}\times x_{qj},\quad \vec{x}_j=\begin{bmatrix}1 & x_{1j} & \dots & x_{rj}\end{bmatrix}, \tag{3}$$

where Φ_{mj} is basis vector calculated by SVD decomposition of stress-strain curve matrix, and w is the number of basis vectors that is extracted from SVD method. The membership degree τ_{ji} (j^{th} input data in i^{th} cluster) is calculated as follows:

$$\tau_{ji}=\frac{\left\|\vec{x}_j-\vec{\mu}_i\right\|_2^{-1}}{\sum_{k=1}^{c}\left\|\vec{x}_j-\vec{\mu}_k\right\|_2^{-1}}, \tag{4}$$

The optimization problem can be formulated as:

$$J=\sum_{j=1}^{n}\left(Output_j-y_j\right)^2+\lambda P^tP=\sum_{j=1}^{n}\left(\sum_{m=0}^{w}F_{mj}\Phi_{mj}-y_j\right)^2+\lambda P^tP,\quad F_{mj}=\sum_{i=1}^{c}\tau_{ij}\sum_{q=0}^{r}p_{miq}x_{qj}, \tag{5}$$

Derivative of Eq. (5) respect to the unknown coefficients p_{miq} is set to zero, and a set of equations is achieved as follows.

$$J=(\Xi P-Y)^T(\Xi P-Y)+\lambda P^tP,\quad \frac{\partial J}{\partial P}=0\rightarrow\left(\Xi^T\Xi+\lambda I\right)P=\Xi^TY \tag{6}$$

where Ξ is defined as follows:

$$\Xi=\begin{bmatrix}
\tau_{11}\Phi_{01} & \dots & \tau_{11}\Phi_{k1} & \dots & \tau_{c1}\Phi_{01} & \dots & \tau_{c1}\Phi_{k1} & \tau_{11}\Phi_{01}x_{11} & \dots & \tau_{c1}\Phi_{w1}x_{11} & \dots & \tau_{11}\Phi_{01}x_{r1} & \dots & \tau_{c1}\Phi_{w1}x_{r1}\\
\tau_{12}\Phi_{12} & \dots & \tau_{12}\Phi_{k2} & \dots & \tau_{c2}\Phi_{12} & \dots & \tau_{c2}\Phi_{k2} & \tau_{12}\Phi_{12}x_{12} & \dots & \tau_{c2}\Phi_{w2}x_{12} & \dots & \tau_{12}\Phi_{12}x_{r1} & \dots & \tau_{c2}\Phi_{w2}x_{r2}\\
\vdots & \dots & \vdots & \dots & \vdots & \dots & \vdots & \vdots & \dots & \vdots & \dots & \vdots & \dots & \vdots\\
\tau_{1j}\Phi_{1j} & \dots & \tau_{1j}\Phi_{kj} & \dots & \tau_{cj}\Phi_{1j} & \dots & \tau_{cj}\Phi_{kj} & \tau_{1j}\Phi_{1j}x_{1j} & \dots & \tau_{cj}\Phi_{wj}x_{1j} & \dots & \tau_{1j}\Phi_{1j}x_{r1} & \dots & \tau_{cj}\Phi_{wj}x_{rj}\\
\vdots & \dots & \vdots & \dots & \vdots & \dots & \vdots & \vdots & \dots & \vdots & \dots & \vdots & \dots & \vdots\\
\tau_{1N}\Phi_{1N} & \dots & \tau_{1N}\Phi_{kN} & \dots & \tau_{cN}\Phi_{1N} & \dots & \tau_{cN}\Phi_{kN} & \tau_{1N}\Phi_{1N}x_{1N} & \dots & \tau_{cN}\Phi_{wN}x_{1N} & \dots & \tau_{1N}\Phi_{1N}x_{rN} & \dots & \tau_{cN}\Phi_{wN}x_{rN}
\end{bmatrix} \tag{7}$$

Table 1
A summary of research on FRP-confined RAC under compressive load.

Ref.	Total number of specimens[a]	Replacement ratios	Applied model	Results
Zhao et al. (Zhao et al., 2015)	18	0, 20	1. Teng et al.'s model (Teng et al., 2009) 2. Jiang and Teng's model (Jiang et al., 2007)	1. Similarity of compressive behavior of NAC and RAC with low replacement ratio 2. Precise predictions for ultimate axial stress by both models 3. Notable discrepancies between the test results and those of both models
Chen et al. (Chen et al., 2018)	24	0, 100	1. Wu and Wei's model (Wu et al., 2016) 2. Jiang and Teng's model (Jiang et al., 2007)	1. Similarity of compressive behavior of NAC and RAC 2. Underestimating the strength and overestimating the ultimate axial strain with lower confinement by Jiang and Teng's (2007) model 3. Accurately predicting post-peak deformation but moderately overestimating compressive strength by Wu and Wei's model
Zhou et al. (Zhou et al., 2016)	48	0, 30, 50, 100	1. Zhou and Wu's (Zhou et al., 2012) 2. Jiang and Teng's model (Jiang et al., 2007)	1. Significant depending compressive behavior of NAC and RAC on the confinement ratio rather than FRP type 2. Slight influence RA replacement ratio on the FRP-confined RAC behavior. 3. Reasonable accuracy in prediction stress-strain curves of FRP-confined RAC along with the ultimate strain and ultimate strength by and Jiang Teng's model and Zhou and Wu's model
Chen et al. (Chen et al., 2016a)	60	0,25,50,75,100	1. Teng et al.'s model (Teng et al., 2009) 2. Jiang and Teng's model (Jiang et al., 2007)	1. The possible need to revise these models with more experimental data 2. Underestimation of compressive strength by both models 3. Overestimation of ultimate strain of FRP confined concrete regardless of replacement ratio by the mentioned models 4. A higher replacement ratio corresponds to lower strength and increased ultimate strain

[a] Similar and duplicate samples have also been counted.

Table 2
Well-known models proposed for FRP-confined concrete under compressive load.

Model	Stress-strain model	Strength model	Strain model
Teng et al.'s model (Teng et al., 2009)	$f_c = E_c\varepsilon_c - \frac{(E_c - E_2)^2}{4f'_{co}}\varepsilon_c^2$ $if\ 0 \le \varepsilon_c \le \varepsilon_{c0},$ $f_c = f'_{co} + E_2\varepsilon_c$ $\text{if} \frac{E_l}{(f'_{co}/\varepsilon_{c0})} \ge 0.01 \text{and } \varepsilon_{c0} \le \varepsilon_c \le \varepsilon_{cu},\ f_c = f'_{co} - \frac{f'_{co} - f'_{cu}}{\varepsilon_{cu} - \varepsilon_{c0}}(\varepsilon_c - \varepsilon_{c0})$ $\text{if} \frac{E_l}{(f'_{co}/\ \varepsilon_{c0})} \le 0.01 \text{ and } \varepsilon_{c0} \le \varepsilon_c \le \varepsilon_{cu}$	$\frac{f'_{cc}}{f'_{co}} = 1 + 3.5\,(\rho_k - 0.01)\,\rho_\varepsilon$	$\frac{\varepsilon_{cu}}{\varepsilon_{c0}} = 1.75 + 6.5\rho_k^{0.8}\ 0.8\rho_\varepsilon^{1.45}$
Jiang and Teng's model (Jiang et al., 2007)	$f_c = \frac{{f'_{cc}}^{*}(\varepsilon_c/\varepsilon_{cc}^{*})r}{r - 1 + (\varepsilon_c/\varepsilon_{cc}^{*})^r}$ $r = \frac{E_c}{E_c - {f'_{cc}}^{*}/\varepsilon_{cc}^{*}}$	$\frac{f'_{cc}}{f'_{co}} = 1 + 3.5\frac{f_l}{f'_{co}}$	$\frac{\varepsilon_{cu}}{\varepsilon_{c0}} = 1 + 17.5\left(\frac{f_l}{f'_{co}}\right)^{1.2}$
Wu and Wei's model (Wu et al., 2016)	$\begin{cases} \frac{f_c}{f'_{cc}} = \frac{x.\lambda}{\lambda - 1 + x^\lambda}, x = \frac{\varepsilon_c}{\varepsilon_{cc}}\ \varepsilon_c < \varepsilon_{cc} \\ \frac{f_c}{f'_{cc}} = 1 + \frac{E_c}{f'_{cc}}\left(\varepsilon_c - \varepsilon_{cc} - \frac{\delta_d^{in}}{L}\right)\ \varepsilon_c > \varepsilon_{cc} \end{cases}$ $\lambda = \frac{E_c}{E_c - \frac{f'_{cc}}{\varepsilon_{cc}}}$	$\frac{f'_{cc}}{f'_{co}} = 1 + 2.2\left(\frac{f_l}{f'_{co}}\right)^{0.94}$	$\frac{\varepsilon_{cu}}{\varepsilon_{c0}} = 1.75 + 140\left(\frac{f_l}{f'_{co}}\right)\varepsilon_{frp}^{0.6}$
Zhou and Wu's model (Zhou et al., 2012)	$f_c = \left[(E_1\varepsilon_n - f_o)e^{-\frac{\varepsilon}{\varepsilon_n}} + f_o + E_2\varepsilon\right]\left(1 - e^{-\frac{\varepsilon}{\varepsilon_n}}\right),$ $\varepsilon_n = n\varepsilon_0$ $\varepsilon_0 = f_0/E_1$	–	–

The proposed model flowchart is depicted in Fig. 3.

4. Modeling

81 experimental test results on FRP-confined concrete with and without recycle aggregates under monotonic axial compression have been collected from eight studies, including those by Zhao et al., 2015) (Zhao et al., 2015), Chen et al., 2018 (Chen et al., 2018), Chen 2016 (Chen et al., 2016a), zhou2016 (Zhou et al., 2016), Lam et al., 2004 (Lam et al., 2004), Lam et al., 2006 (Lam et al., 2006), Teng et al., 2007 (Teng et al., 2007), Jiang et al., 2007 (Jiang et al., 2007). Zhou et al. (2016) investigated RCA derived from local construction concrete waste, with a particle size range of 5–31.5 mm. The apparent density was reported as 2476.9 kg/m^3, while the stacking density was 1158.2 kg/m^3. The water absorption rate was relatively high at 6.31 %, and the crushing index was 18.6 %. Zhao et al. (2015)studied RCA sourced from a local recycling plant, specifically aggregates of 10 mm and 20 mm in size. However, only the water absorption rate was reported, which was 5.34 %, with no additional details on density or crushing properties. Chen et al. (2016a)examined RCA provided by a professional local company, where the original concrete was obtained from a single source. The particle size ranged from 4 mm to 20 mm, with a recorded water absorption rate of 4.4 %. However, no data on density or crushing index was available. Chen et al. (2018)analyzed RCA supplied by a commercial supplier in Shenzhen (Lvfar Group), with a particle size range of 5–20 mm. The water absorption rate was found to be 3.19 %, and the oven-dry density was 1459 kg/m^3. Other parameters were not reported. Tables 1 and 2 summary details of some well-known models.

The experiments focused on specimens with fibers oriented in the

Table 3
Experimental database of FRP–confined ARC.

Ref.	Label	$D(mm)$	$H(mm)$	E_{frp}(GPa)	ε_{FRP}(%)	$t_{FRP}(mm)$	$\acute{f}_{c0}$(MPa)	R(%)
J. L. Zhao et al., 2015	S1	153	305	–	–	–	45	0
	S2	153	305	98.7	1.720	0.17	45	0
	S3	153	305	98.7	1.720	0.34	45	0
	S4	153	305	98.7	1.720	0.51	45	0
	S5	153	305	98.7	1.720	0	44.9	20
	S6	153	305	98.7	1.720	0.17	44.9	20
	S7	153	305	98.7	1.720	0.34	44.9	20
	S8	153	305	98.7	1.720	0.51	44.9	20
	S9	153	305	98.7	1.720	0	37.3	100
	S10	153	305	98.7	1.720	0.17	37.3	100
	S11	153	305	98.7	1.720	0.34	37.3	100
	S12	153	305	98.7	1.720	0.51	37.3	100
Chen et al., 2018	S13	150	300	244	4.104	0.111	45.8	0
	S14	150	300	244	4.104	0.222	45.8	0
	S15	150	300	244	4.104	0.333	45.8	0
	S16	200	400	244	4.104	0.111	44.3	0
	S17	200	400	244	4.104	0.222	44.3	0
	S18	200	400	244	4.104	0.333	44.3	0
	S19	300	600	244	4.104	0.111	43.6	0
	S.20	300	600	244	4.104	0.222	43.6	0
	S21	300	600	244	4.104	0.333	43.6	0
	S22	150	300	244	4.104	0.111	41.6	100
	S23	150	300	244	4.104	0.222	41.6	100
	S24	150	300	244	4.104	0.333	41.6	100
	S25	200	400	244	4.104	0.111	41.5	100
	S26	200	400	244	4.104	0.222	41.5	100
	S27	200	400	244	4.104	0.333	41.5	100
	S28	300	600	244	4.104	0.111	38.8	100
	S29	300	600	244	4.104	0.222	38.8	100
	S30	300	600	244	4.104	0.333	38.8	100
Chen 2016	S31	150	300	–	–	–	44.44	0
	S32	150	300	250	3.450	0.111	44.44	0
	S33	150	300	250	3.225	0.222	44.44	0
	S34	150	300	250	3.183	0.333	44.44	0
	S35	150	300	0	0.000	0	40.75	25
	S36	150	300	250	3.167	0.111	40.75	25
	S37	150	300	250	3.383	0.222	40.75	25
	S38	150	300	250	2.858	0.333	40.75	25
	S39	150	300	0	0.000	0	37.03	50
	S40	150	300	250	3.317	0.111	37.03	50
	S41	150	300	250	3.258	0.222	37.03	50
	S42	150	300	250	3.050	0.333	37.03	50
	S43	150	300	0	0.000	0	37.48	75
	S44	150	300	250	3.533	0.111	37.48	75
	S45	150	300	250	3.592	0.222	37.48	75
	S46	150	300	250	2.767	0.333	37.48	75
	S47	150	300	0	0.000	0	32.87	100
	S48	150	300	250	3.333	0.111	32.87	100
	S49	150	300	250	3.383	0.222	32.87	100
	S50	150	300	250	2.883	0.333	32.87	100
zhou2016	S51	150	300	272.73	3.930	0.167	48.41	0
	S52	150	300	272.73	3.930	0.501	48.41	0
	S53	150	300	272.73	3.930	0.167	42.74	30
	S54	150	300	272.73	3.930	0.501	42.74	30
	S55	150	300	272.73	3.930	0.167	43.06	50
	S56	150	300	272.73	3.930	0.501	43.06	50
	S57	150	300	272.73	3.930	0.501	37.21	100
	S58	150	300	272.73	3.930	0.167	40.54	100
	S59	150	300	272.73	3.930	0.501	40.54	100
	S60	150	300	272.73	3.930	0.501	56.34	100
Lam and Teng 2004	S61	152	305	250.5	2.586	0.165	35.9	0
	S62	152	305	250.5	2.453	0.33	35.9	0
	S63	152	305	250.5	2.214	0.495	34.3	0
	S64	152	305	21.8	0.363	1.27	38.5	0
	S65	152	305	21.8	0.374	2.54	38.5	0
Lam et al., 2006	S66	152	305	250	2.467	0.165	41.1	0
	S67	152	305	247	2.454	0.33	38.9	0
Teng et al., 2007	S68	152	305	80.1	1.393	0.17	39.6	0
	S69	152	305	80.1	1.642	0.34	39.6	0
	S70	152	305	80.1	1.451	0.51	39.6	0

(continued on next page)

Table 3 (*continued*)

Ref.	Label	$D(mm)$	$H(mm)$	E_{frp}(GPa)	ε_{FRP}(%)	$t_{FRP}(mm)$	$\acute{f}_{c0}$(MPa)	R(%)
T. Jiang et al., 2007	S71	152	305	80.1	1.537	0.17	33.1	0
	S72	152	305	80.1	1.377	0.17	45.9	0
	S73	152	305	80.1	1.377	0.34	45.9	0
	S74	152	305	80.1	1.415	0.51	45.9	0
	S75	152	305	240.7	2.337	0.68	38	0
	S76	152	305	240.7	2.189	1.02	38	0
	S77	152	305	240.7	2.105	1.36	38	0
	S78	152	305	260	2.635	0.11	37.7	0
	S79	152	305	260	2.214	0.11	44.2	0
	S80	152	305	260	2.759	0.22	44.2	0
	S81	152	305	250.5	2.585	0.33	47.6	0

Table 4
Summary of databases of FRP-confined ARC.

	$D(mm)$	$H(mm)$	E_{frp}(GPa)	ε_{FRP}(%)	$t_{FRP}(mm)$	$\acute{f}_{c0}$(MPa)	R(%)
Min	150	300	0	0	0	32.87	0
Max	300	600	272.73	4.1040	2.54	56.34	100
Average	165.7778	331.6667	193.3222	2.7212	0.3135	41.0952	36.2963

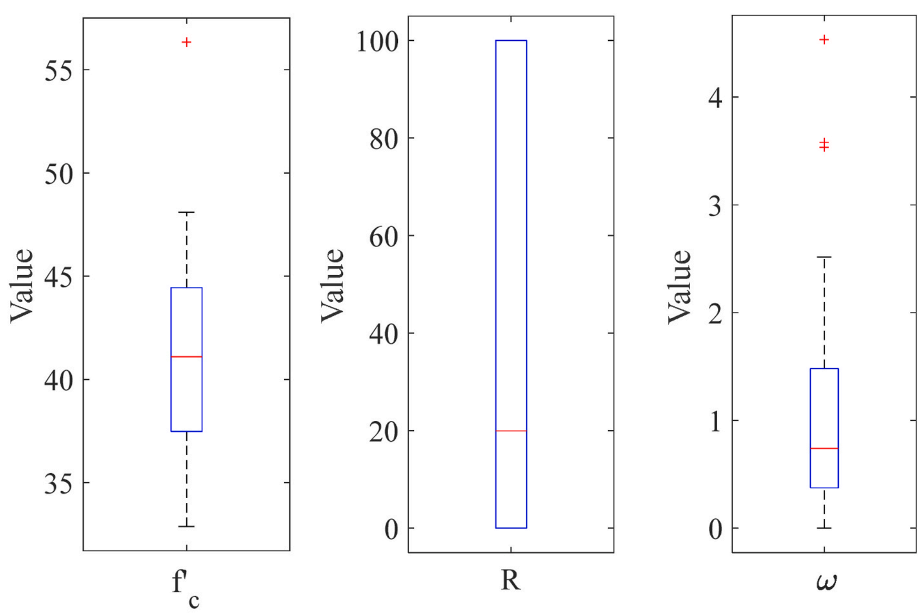

Fig. 4. The boxplots of $\acute{f}_c$, R, and ω

hoop direction. Table 3 provides the parameters of experimental test used to develop the proposed models. The parameter D represents the diameter (in mm), H is the height (in mm), E_{FRP} denotes the FRP elasticity modulus (in GPa), ε_{FRP} is the ultimate strain of the FRP, $\acute{f}_{c0}$ refers to the concrete strength (in MPa), and R indicates the percentage of aggregate replacement with recycled materials.

Table 4 tabulates the range of gathered input parameters for FRP-confined RAC under compression load.

The curves are digitized, converting the graphical diagrams into numerical values. A consistent strain increment of 0.0005 was applied across all curves to maintain uniformity in data sampling. This process resulted in the collection of 2452 data points, which were then used for further analysis. 400 data points are randomly selected for testing, and the remaining data are used to train the system. The coefficient λ is set to the value of 0.05. The number of clusters and basis vectors were both set to a value of 3 for the analysis.

In existing models developed for confined concrete, compressive strength and the confinement pressure applied by the composite jacket have been identified as the most critical parameters influencing the stress-strain diagram. Nearly all previous models have incorporated these two parameters, either directly or indirectly. Additionally, in the present study, we aim to investigate the effect of the percentage of recycled aggregates on the prediction of stress-strain curves. While other parameters could also be considered, our objective was to develop and train the model with a minimal number of input parameters. Thus, the system input parameters are f_c', R, and the parameter ω is defined as follows.

$$\omega = \frac{E_{frp} \times \varepsilon_{FRP} \times t_{FRP}}{D} \tag{8}$$

The box plot of the system's input parameters is shown in Fig. 4. Three clusters and three basis vectors are considered to structure the proposed method, as shown in Fig. 5a and b, respectively. Cluster centers are as follows.

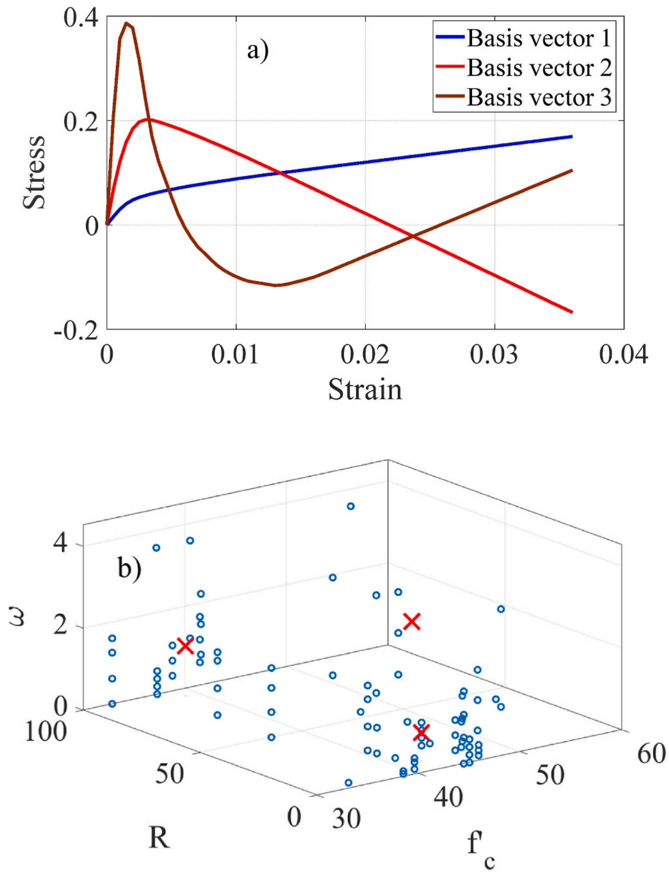

Fig. 5. a) Basis vectors, b) Cluster centers (marked with a red cross).

$$\vec{\mu}_1 = [38.7677 \quad 94.2308 \quad 1.2210]$$
$$\vec{\mu}_2 = [42.2302 \quad 8.5417 \quad 0.6988]$$
$$\vec{\mu}_3 = [41.9571 \quad 11.4286 \quad 3.3638]$$

The cross plot comparing predicted and experimental stress values in Fig. 6, indicates strong predictive performance, supported by key statistical metrics. An R2 value of (training = 0.975, testing = 0.960) suggests a robust correlation between predicted and observed data. The model's accuracy is further reflected in an A-20 score of (training = 0.973, testing = 0.968) and a Variance Accounted For (VAF) of (training = 97.54 %, testing = 95.96 %). With an RMSE of (training = 4.066, testing = 4.404), the prediction error remains low, confirming that the model aligns closely with the experimental data.

In Fig. 7, both a) the frequency analysis and b) the error distribution of stresses are illustrated based on 2452 data points. It can be observed that the error distribution follows a normal pattern, with the majority of the data points having errors close to zero.

5. Results and discussion

Although the proposed model demonstrates good predictive performance, it remains a 'black-box' model due to its lack of transparency and interpretability. To address this, we apply an interpretable method called Shapley Additive Explanations (SHAP) to better understand the inner workings of the XGBoost model and identify the most important features. SHAP, based on game theory, quantifies the contribution of each variable to the model's predictions. It uses Shapley values to assign credit to individual features, which are calculated by considering all possible combinations of features. A coalition is a subset of features involved in generating a prediction. The Shapley value shows the average contribution of a feature across all coalitions. In Fig. 8, a SHAP summary plot is utilized to illustrate the impact of each feature on stress value at low and high strain based on the provided data samples. Each point on the summary plot corresponds to an individual instance (i.e., a data sample), along with its associated SHAP value and the relevant feature. The color gradient represents the feature values, transitioning from the lowest (blue) to the highest (yellow). Fig. 8 illustrates that the unconfined concrete compressive strength is the most significant factor

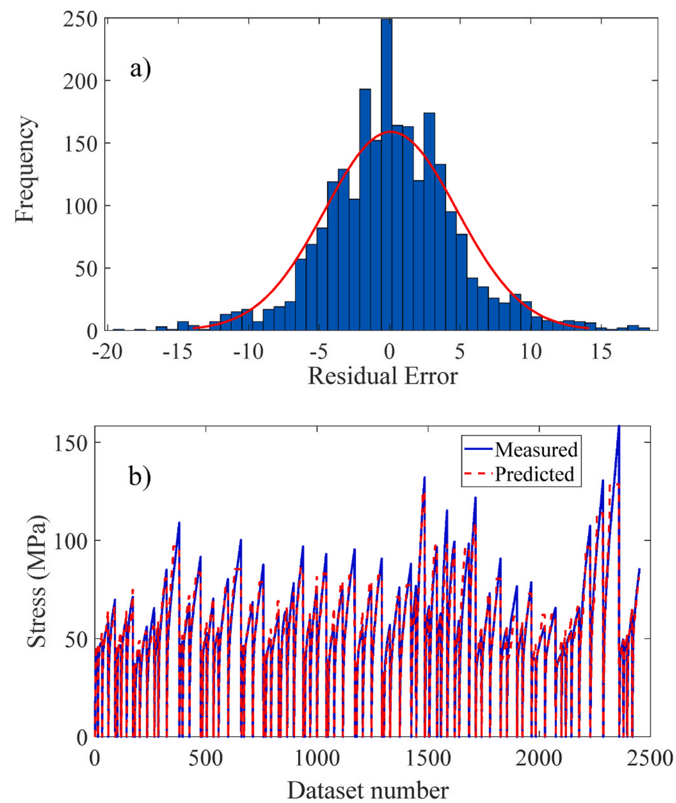

Fig. 7. a) Frequency analysis and b) error distribution of stresses.

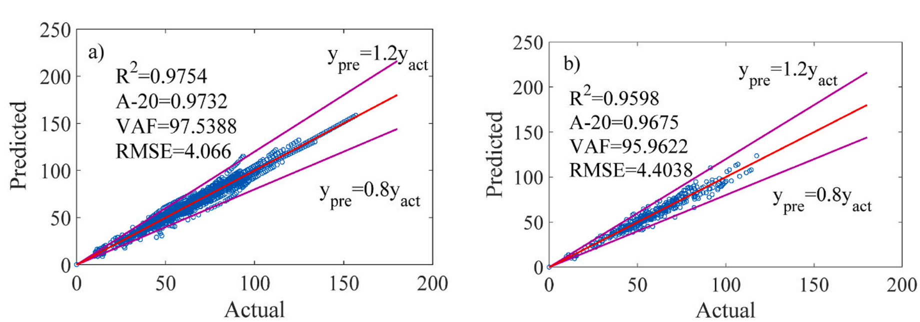

Fig. 6. Scatter plot of predicted stress values versus experimental laboratory values; a) train dataset, b) test dataset.

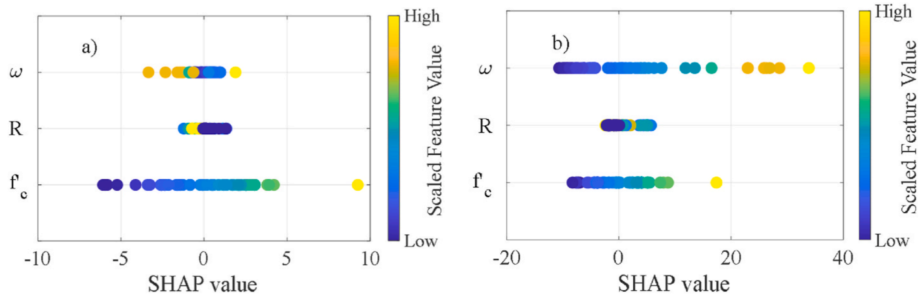

Fig. 8. A summary of SHAP results for different features. Stress at a) low strain and b) high strain.

affecting stress levels at low strains. Additionally, at high strains, confinement has a substantial impact on the stress level at a given strain. Moreover, the proportion of recycled materials has a lesser effect compared to the other two parameters in both low and high strain ranges.

Fig. 9 illustrates a comparison between the experimental curves with the results from some popular existing models. The results of previous models extracted from related literature mentioned in Table 3. It can be observed that the differences between the stress-strain curves of previous models and the experimental data are sometimes significant. However, the results of the proposed method are more precise and closely match the experimental curves, demonstrating its accuracy in representing the behavior of concrete confined with composite sheets containing RA.

Gray correlation coefficient analysis is a technique used to evaluate the relation between variables and quantify their correlation. The main steps of this method with considering two normalized sequences $X_i' = (x_i(1), x_i(2), \ldots, x_i(m))$ and $Y_j' = \left(y_j(1), y_j(2), \ldots, y_j(m)\right)$. The procedures employed to determine the gray correlation degree are as follows (Zhu et al., 2021; Yu et al., 2024):

1. Computing the sequence of differences:

$$\Delta_i(k) = \left|Y_j'(k) - X_i'(k)\right|, (k = 1, 2, \ldots, m) \tag{9}$$

2. Determining the maximum and minimum differences between two poles:

$$M = \underset{i}{max}\underset{k}{max}\Delta_i(k), N = \underset{i}{min}\underset{k}{min}\Delta_i(k) \tag{10}$$

3. Computing the correlation coefficients:

$$\gamma_{ji}(k) = \frac{N + \xi M}{\Delta_i(k) + \xi M}, \xi \in (0, 1) \tag{11}$$

where $\xi \in (0, 1)$ is typically assigned a value between 0.3 and 0.7.

4. Computing the gray correlation degree:

$$\gamma_{ji} = \frac{1}{m}\sum_{k=1}^{m}\gamma_{ji}(k), (i = 1, 2, \ldots, n), \tag{12}$$

Where m represents the number of samples, and n denotes the number of related factor sequences.

Gray correlation coefficient between inputs (f_c', R, ω) and the maximum stress is 0.7348, 0.6157, and 0.8718, respectively. Based on the calculated these coefficients, it can be observed that the third input exhibits the strongest correlation with the output, with a value of 0.8718. This indicates a very strong relationship between the third input and the output, suggesting that this input plays a crucial role in predicting or determining the output. The first input also shows a relatively strong correlation (0.7348), indicating its significant influence. However, the second input, with a correlation of 0.6157, demonstrates a moderate relationship with the output.

6. A simple empirical stress-strain model

In this study, a simple empirical relationship is also developed to predict the stress-strain curves of FRP-confined recycled aggregate concrete under compression loading. Initially, the principal vector was extracted from experimental stress-strain curves using Singular Value Decomposition (SVD). This principal vector captured the key features of the material's behavior under compression and was subsequently approximated using a sixth-degree polynomial function to model the nonlinear stress-strain relationship. Typically, the stress–strain response of confined concrete exhibits a bilinear trend: an initial ascending branch with a relatively steep slope, followed by a strain-hardening stage with a more moderate slope. These two regions are smoothly connected, reflecting the progressive transition from unconfined-like response to confinement-dominated behavior. The shape of the primary basis vector captures this bilinear yet continuous pattern, thereby representing the fundamental compressive mechanism of FRP-confined RAC. Fig. 10 demonstrates the accuracy of the proposed polynomial equation in approximating this basis vector. It should be noted that, since the model primarily exhibits a bilinear form with an ascending second branch, prediction errors may increase under low confinement conditions. For such cases, incorporating the second basis vector is recommended to capture the response more accurately.

Then, a linear relationship between the compressive strength of concrete, lateral confinement pressure, and the percentage of recycled materials is established according to the following equation.

$$\begin{aligned} &\sigma = \left(\alpha_0 + \alpha_{f_c'} * f_c' + \alpha_R * R + \alpha_\omega * \omega\right)\varphi_1 \\ &\varphi_1 = -2.7672\times10^9 \times \varepsilon^6 + 3.3223\times10^8 \times \varepsilon^5 - 1.561\times10^7 \times \varepsilon^4 + 3.6283\times10^5 \times \varepsilon^3 - 4.3456\times10^3 \times \varepsilon^2 + 28.374 \times \varepsilon, \varepsilon < 0.035 \end{aligned} \tag{13}$$

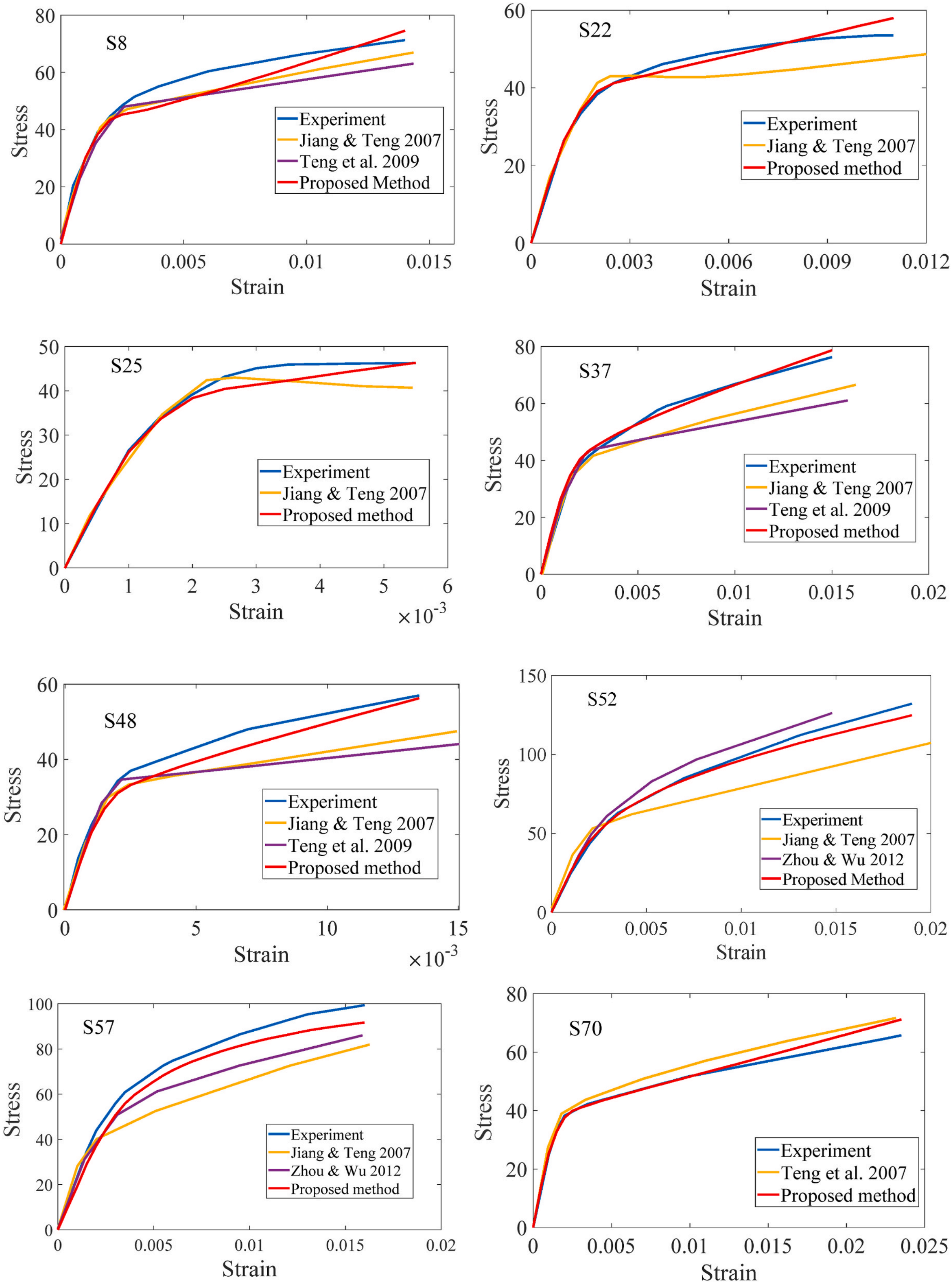

Fig. 9. Comparison of the experimental curves with the results from some previous models.

The condition $\varepsilon < 0.035$ is imposed because all experimental datasets used in this study showed maximum compressive strains below this threshold. Since the polynomial fitting is highly nonlinear and was only trained within this range, extrapolation beyond $\varepsilon = 0.035$ would not be reliable. Moreover, since the optimization of the coefficients was conducted on datasets covering RAC replacement rates from 0 % to 100 %, the proposed model is applicable across the full range of RAC replacement rates.

The unknown parameters of empirical relationship is optimized using the least squares method, minimizing the discrepancy between the predicted and experimental stress-strain curves. The optimized param-

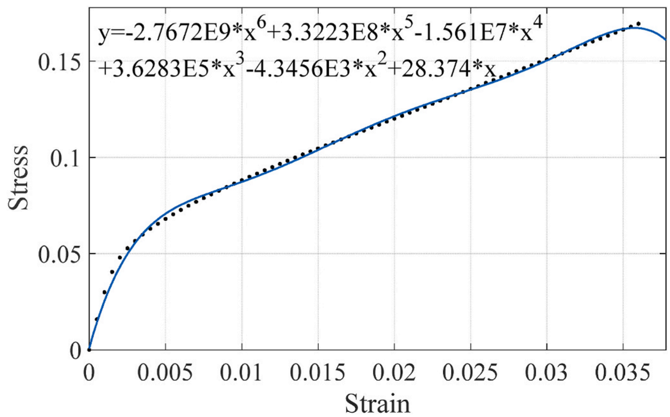

Fig. 10. Approximating the first basis vector using a sixth-degree polynomial function.

eters are $\alpha_0 = 118.3, \alpha_{\acute{f}_c} = 11.81, \alpha_R = -0.167, \alpha_\omega = 91.1$. As can be observed, the negative coefficient of the recycled material substitution percentage indicates the negative impact of this parameter on the stress-strain curves.

The performance of the proposed model was further validated by comparing it with two widely used models (Teng et al.'s model (Teng et al., 2009) and Zhou and Wu's model (Zhou et al., 2012)) through cross-plots, as illustrated in Fig. 11. In both models, $E_c = 4700\sqrt{f_{co}}$ was adopted as the initial elastic modulus. In the Zhou and Wu's model (Zhou et al., 2012), the parameter $n = 3$ was assumed as the shape factor. The comparison was conducted over the entire dataset comprising 81 experimental stress–strain curves discretized into 2452 data points. Quantitative evaluation was based on the coefficient of determination (R^2) and the Root Mean Square Error (RMSE). The results reveal that the proposed model consistently outperforms the existing models, achieving the highest accuracy ($R^2 = 0.925$) and the lowest prediction error (RMSE = 6.07), despite relying on only four unknown parameters. These findings provide strong evidence for the robustness and efficiency of the proposed model, as well as its superiority over the competing approaches.

Fig. 12 presents a comparison between the predicted and experimental stress–strain curves for specimens with low, medium, and high RAC replacement ratios.

7. Limitations and future works

Although this research aimed to incorporate a more diverse range of experimental tests compared to previous studies, there is still a pressing need for additional experimental data to enhance the robustness of the model. The variability in recycled aggregate properties, including factors such as type, size, and composition, may significantly reduce the output scatter and lead to more accurate model predictions. Addressing these factors would likely refine the model and increase its precision.

The model developed in this study specifically targets confined recycled aggregate concrete, yet the proposed technique has broader potential. It can be adapted to predict other experimental behaviors across various fields, offering a flexible approach for different material systems. The general applicability of this methodology makes it useful for extending beyond the scope of this study, contributing to advancements in predictive modeling for a wide range of engineering and material sciences.

8. Conclusions

Given the importance of applying recycled aggregates in concrete and the lack of accuracy in previous methods for modeling the behavior of FRP-confined ARC, we were motivated to introduce, for the first time,

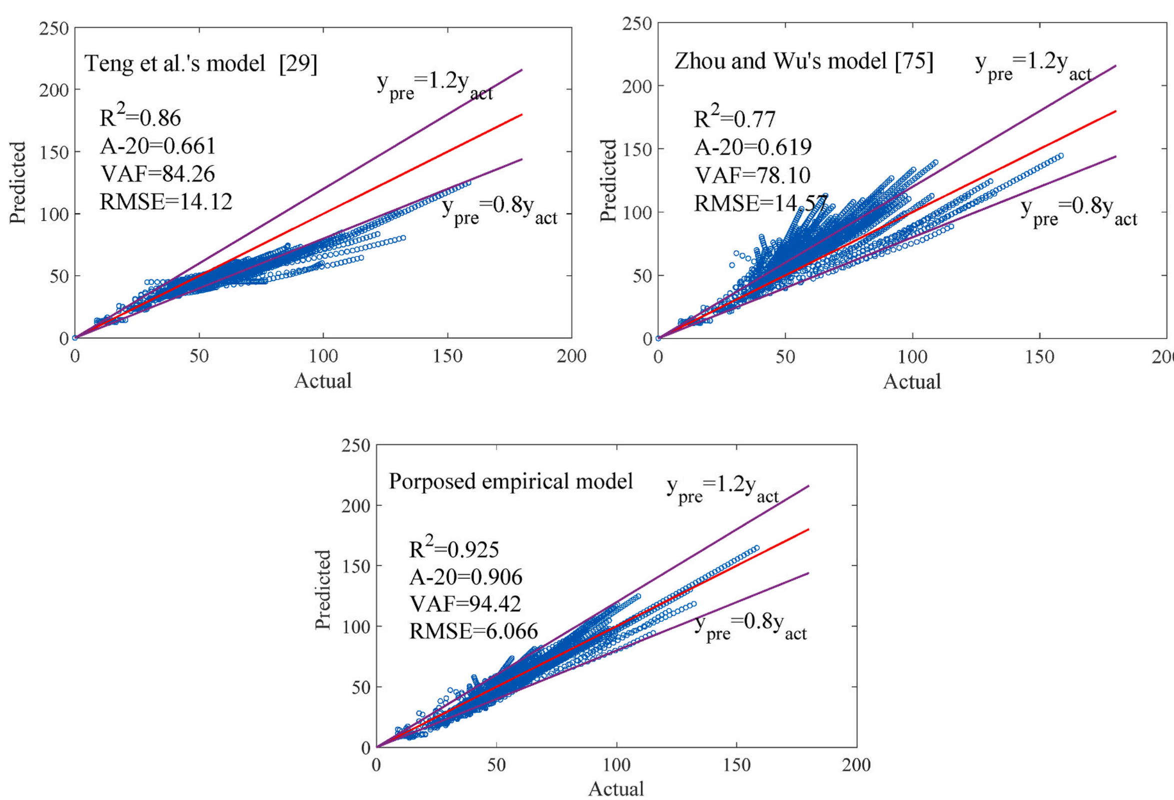

Fig. 11. Scatter plot of predicted stress values versus experimental laboratory values.

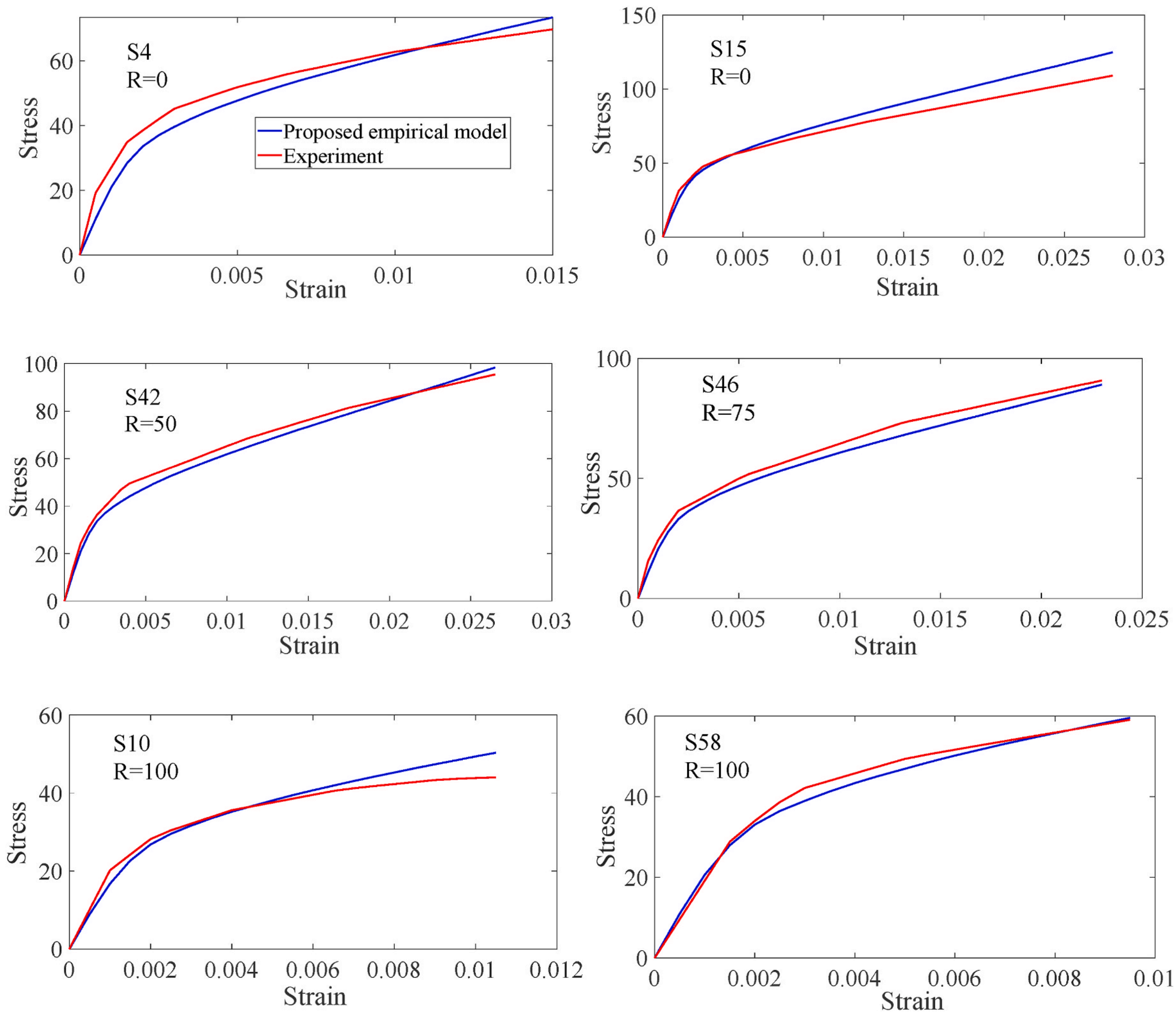

Fig. 12. Performance of the proposed model for low, medium, and high RAC replacement ratios.

an ML-based method for this type of concrete. A collection of 81 stress-strain curves was gathered from eight distinct sources, resulting in the digitization of 2452 data points at a strain rate of 0.0005 for training the proposed model. The effectiveness of the approach was verified through comparison with various experimental datasets, allowing for a comprehensive analysis of how different parameters affect the stress-strain behavior. Based on this research, following conclusion can be drawn.

- At low strain levels, the unconfined compressive concrete strength has the most significant effect on the stress at the same strain.
- At higher strains, confinement becomes the dominant factor, with increasing confinement leading to higher stress at corresponding strain levels.
- The addition of recycled aggregates in very high percentages can reduce the stress sustained at equivalent strain levels.
- The model developed in this research has successfully predicted the behavior of FRP-confined concrete with recycled aggregates under compression, demonstrating its effectiveness in capturing the unique mechanical properties of this material.

CRediT authorship contribution statement

Hossein Saberi: Writing – review & editing, Writing – original draft, Visualization, Validation, Supervision, Software, Resources, Project administration, Methodology, Investigation, Funding acquisition, Formal analysis, Data curation, Conceptualization. **Hamid Saberi:** Writing – review & editing, Writing – original draft, Visualization.

Funding

This research was supported by Alexander von Humboldt Foundation. Publishing fees supported by Funding Programme Open Access Publishing of Hamburg University of Technology (TUHH).

Declaration of competing interest

The authors declare that they have no known competing financial interests or personal relationships that could have appeared to influence the work reported in this paper.

Data availability

Data will be made available on request.

References

Abdollahzadeh, G., Jahani, E., Kashir, Z., 2016. Predicting of compressive strength of recycled aggregate concrete by genetic programming. Comput. Concrete 18 (2), 155–163.

Akhtar, A., Sarmah, A.K., 2018. Construction and demolition waste generation and properties of recycled aggregate concrete: a global perspective. J. Clean. Prod. 186, 262–281.

Armaghani, D.J., et al., 2024. Toward precise long-term rockburst forecasting: a fusion of SVM and cutting-edge meta-heuristic algorithms. Nat. Resour. Res. 1–26.

Askari, S., et al., 2017. Generalized entropy based possibilistic fuzzy C-Means for clustering noisy data and its convergence proof. Neurocomputing 219, 186–202.

Asteris, P.G., Nikoo, M., 2019a. Artificial bee colony-based neural network for the prediction of the fundamental period of infilled frame structures. Neural Comput. Appl. 31 (9), 4837–4847.

Asteris, P.G., Kolovos, K.G., 2019b. Self-compacting concrete strength prediction using surrogate models. Neural Comput. Appl. 31 (Suppl. 1), 409–424.

Asteris, P.G., et al., 2024. Predicting uniaxial compressive strength of rocks using ANN models: incorporating porosity, compressional wave velocity, and schmidt hammer data. Ultrasonics 141, 107347.

Cevik, A., Guzelbey, I.H., 2008. Neural network modeling of strength enhancement for CFRP confined concrete cylinders. Build. Environ. 43 (5), 751–763.

Chen, Z., et al., 2014. Bond behaviors of shape steel embedded in recycled aggregate concrete and recycled aggregate concrete filled in steel tubes. Steel Compos. Struct. 17 (6), 929–949.

Chen, G., et al., 2016a. Behavior of CFRP-confined recycled aggregate concrete under axial compression. Constr. Build. Mater. 111, 85–97.

Chen, Z., et al., 2016b. Recycling and reuse of construction and demolition waste in concrete-filled steel tubes: a review. Constr. Build. Mater. 126, 641–660.

Chen, G., et al., 2018. Compressive behavior of CFRP-confined recycled aggregate concrete in different-sized circular sections. J. Compos. Construct. 22 (4), 04018021.

Chen, Y., et al., 2019. Performance evaluation of recycled aggregate concrete under multiaxial compression. Constr. Build. Mater. 229, 116935.

Corinaldesi, V., 2010. Mechanical and elastic behaviour of concretes made of recycled-concrete coarse aggregates. Constr. Build. Mater. 24 (9), 1616–1620.

Dantas, A.T.A., Leite, M.B., de Jesus Nagahama, K., 2013. Prediction of compressive strength of concrete containing construction and demolition waste using artificial neural networks. Constr. Build. Mater. 38, 717–722.

Deng, F., et al., 2018. Compressive strength prediction of recycled concrete based on deep learning. Constr. Build. Mater. 175, 562–569.

Duan, Z.-H., Kou, S.-C., Poon, C.-S., 2013a. Prediction of compressive strength of recycled aggregate concrete using artificial neural networks. Constr. Build. Mater. 40, 1200–1206.

Duan, Z.-H., Kou, S.-C., Poon, C.-S., 2013b. Using artificial neural networks for predicting the elastic modulus of recycled aggregate concrete. Constr. Build. Mater. 44, 524–532.

Duan, J., et al., 2021. A novel artificial intelligence technique to predict compressive strength of recycled aggregate concrete using ICA-XGBoost model. Eng. Comput. 37, 3329–3346.

Elsanadedy, H., et al., 2012. Prediction of strength parameters of FRP-confined concrete. Compos. B Eng. 43 (2), 228–239.

Fathifazl, G., et al., 2011. Creep and drying shrinkage characteristics of concrete produced with coarse recycled concrete aggregate. Cement Concr. Compos. 33 (10), 1026–1037.

Fattahi, H., Ghaedi, H., Armaghani, D.J., 2024. Optimizing fracture toughness estimation for rock structures: a soft computing approach with GWO and IWO algorithms. Measurement 238, 115306.

Ferreira, L., De Brito, J., Barra, M., 2011. Influence of the pre-saturation of recycled coarse concrete aggregates on concrete properties. Mag. Concr. Res. 63 (8), 617–627.

Gholampour, A., Ozbakkaloglu, T., 2018. Time-dependent and long-term mechanical properties of concretes incorporating different grades of coarse recycled concrete aggregates. Eng. Struct. 157, 224–234.

Ho, H.-J., Iizuka, A., Shibata, E., 2021. Chemical recycling and use of various types of concrete waste: a review. J. Clean. Prod. 284, 124785.

Hosseini, S., et al., 2024. Fuzzy cognitive map for evaluating critical factors causing rockbursts in underground construction: a fundamental Study. Rock Mech. Rock Eng. 1–26.

Huang, G.-B., Wang, D.H., Lan, Y., 2011. Extreme learning machines: a survey. International journal of machine learning and cybernetics 2, 107–122.

Jalal, M., Ramezanianpour, A.A., 2012. Strength enhancement modeling of concrete cylinders confined with CFRP composites using artificial neural networks. Compos. B Eng. 43 (8), 2990–3000.

Jamali, F., et al., 2022. Prediction of compressive strength of fiber-reinforced polymers-confined cylindrical concrete using artificial intelligence methods. J. Reinforc. Plast. Compos. 41 (17–18), 679–704.

Jiang, T., Teng, J., 2007. Analysis-oriented stress–strain models for FRP–confined concrete. Eng. Struct. 29 (11), 2968–2986.

Kamgar, R., et al., 2020. A proposed soft computing model for ultimate strength estimation of FRP-confined concrete cylinders. Appl. Sci. 10 (5), 1769.

Kang, T.H.-K., et al., 2014. Flexural testing of reinforced concrete beams with recycled concrete aggregates. ACI Struct. J. 111 (3).

Keshtegar, B., et al., 2021. Hybrid regression and machine learning model for predicting ultimate condition of FRP-confined concrete. Compos. Struct. 262, 113644.

Khademi, F., et al., 2016a. Predicting strength of recycled aggregate concrete using artificial neural network, adaptive neuro-fuzzy inference system and multiple linear regression. Int. J. Sustain. Built Environ. 5 (2), 355–369.

Khademi, F., Jamal, S.M., 2016b. Predicting the 28 days compressive strength of concrete using artificial neural network. i-manager's Journal on Civil Engineering 6 (2), 1.

Khosravi, K., et al., 2018a. Quantifying hourly suspended sediment load using data mining models: case study of a glacierized Andean catchment in Chile. J. Hydrol. 567, 165–179.

Khosravi, K., Panahi, M., Tien Bui, D., 2018b. Spatial prediction of groundwater spring potential mapping based on an adaptive neuro-fuzzy inference system and metaheuristic optimization. Hydrol. Earth Syst. Sci. 22 (9), 4771–4792.

Kumar, A., et al., 2022. Compressive strength prediction of lightweight concrete: machine learning models. Sustainability 14 (4), 2404.

Kumar, A., et al., 2023. Prognosis of compressive strength of fly-ash-based geopolymer-modified sustainable concrete with ML algorithms. Struct. Concr. 24 (3), 3990–4014.

Lam, L., Teng, J., 2004. Ultimate condition of fiber reinforced polymer-confined concrete. J. Compos. Construct. 8 (6), 539–548.

Lam, L., et al., 2006. FRP-confined concrete under axial cyclic compression. Cement Concr. Compos. 28 (10), 949–958.

Liao, J., et al., 2021. Compressive behavior of FRP-confined ultra-high performance concrete (UHPC) in circular columns. Eng. Struct. 249, 113246.

Liao, J., et al., 2022. Design-oriented stress-strain model for FRP-confined ultra-high performance concrete (UHPC). Constr. Build. Mater. 318, 126200.

Liao, J., et al., 2023. FRP-confined concrete columns with a stress reduction-recovery behavior: a state-of-the-art review, design recommendations and model assessments. Compos. Struct. 321, 117313.

Liu, T., et al., 2020. Freeze-thaw damage evolution of fractured rock mass using nuclear magnetic resonance technology. Cold Reg. Sci. Technol. 170, 102951.

Naderpour, H., Rafiean, A.H., Fakharian, P., 2018. Compressive strength prediction of environmentally friendly concrete using artificial neural networks. J. Build. Eng. 16, 213–219.

Nagataki, S., et al., 2004. Assessment of recycling process induced damage sensitivity of recycled concrete aggregates. Cement Concr. Res. 34 (6), 965–971.

Olorunsogo, F., Padayachee, N., 2002. Performance of recycled aggregate concrete monitored by durability indexes. Cement Concr. Res. 32 (2), 179–185.

Omran, B.A., Chen, Q., Jin, R., 2016. Comparison of data mining techniques for predicting compressive strength of environmentally friendly concrete. J. Comput. Civ. Eng. 30 (6), 04016029.

Ozbakkaloglu, T., Gholampour, A., Xie, T., 2018. Mechanical and durability properties of recycled aggregate concrete: effect of recycled aggregate properties and content. J. Mater. Civ. Eng. 30 (2), 04017275.

Padmini, A., Ramamurthy, K., Mathews, M., 2009. Influence of parent concrete on the properties of recycled aggregate concrete. Constr. Build. Mater. 23 (2), 829–836.

Pedro, D., De Brito, J., Evangelista, L., 2015. Performance of concrete made with aggregates recycled from precasting industry waste: influence of the crushing process. Mater. Struct. 48, 3965–3978.

Pham, T.M., Hadi, M.N., 2014. Predicting stress and strain of FRP-confined square/rectangular columns using artificial neural networks. J. Compos. Construct. 18 (6), 04014019.

Rezaei, M., et al., 2024. Improved determination of the S-wave velocity of rocks in dry and saturated conditions: application of machine-learning algorithms. Transportation Geotechnics 49, 101371.

Saberi, H., Rahai, A., Hatami, F., 2017. A fast and efficient clustering based fuzzy time series algorithm (FEFTS) for regression and classification. Appl. Soft Comput. 61, 1088–1097.

Saberi, H., Sharbati, R., Farzanegan, B., 2022. A gradient ascent algorithm based on possibilistic fuzzy C-Means for clustering noisy data. Expert Syst. Appl. 191, 116153.

Silva, R., de Brito, J., Dhir, R., 2015. The influence of the use of recycled aggregates on the compressive strength of concrete: a review. European Journal of Environmental and Civil Engineering 19 (7), 825–849.

Tam, V.W., Gao, X., Tam, C.M., 2005. Microstructural analysis of recycled aggregate concrete produced from two-stage mixing approach. Cement Concr. Res. 35 (6), 1195–1203.

Teng, J., et al., 2007. Hybrid FRP–concrete–steel tubular columns: concept and behavior. Constr. Build. Mater. 21 (4), 846–854.

Teng, J., et al., 2009. Refinement of a design-oriented stress–strain model for FRP-confined concrete. J. Compos. Construct. 13 (4), 269–278.

Topçu, İ.B., Sarıdemir, M., 2008. Prediction of mechanical properties of recycled aggregate concretes containing silica fume using artificial neural networks and fuzzy logic. Comput. Mater. Sci. 42 (1), 74–82.

Wang, J., Lin, S., Zhao, Y.-G., 2024. Stress path-based compressive strength model of FRP-confined recycled aggregate concrete. Constr. Build. Mater. 440, 137437.

Wu, B., et al., 2013. Cyclic testing of thin-walled circular steel tubular columns filled with demolished concrete blocks and fresh concrete. Thin-Walled Struct. 66, 50–61.

Wu, Y.-F., Wei, Y., 2016. Stress–strain modeling of concrete columns with localized failure: an analytical study. J. Compos. Construct. 20 (3), 04015071.

Xiao, J., et al., 2012. Crack propagation in recycled aggregate concrete under uniaxial compressive loading. ACI Mater. J. 109 (4).

Xu, J.-J., et al., 2017a. Recycled aggregate concrete in FRP-confined columns: a review of experimental results. Compos. Struct. 174, 277–291.

Xu, J.-J., et al., 2017b. Simulation of seismic behavior of square recycled aggregate concrete–filled steel tubular columns. Constr. Build. Mater. 149, 553–566.

Xu, J., et al., 2019. Parametric sensitivity analysis and modelling of mechanical properties of normal-and high-strength recycled aggregate concrete using grey theory, multiple nonlinear regression and artificial neural networks. Constr. Build. Mater. 211, 479–491.

Younis, K.H., Pilakoutas, K., 2013. Strength prediction model and methods for improving recycled aggregate concrete. Constr. Build. Mater. 49, 688–701.

Yu, Y., et al., 2024. An agile, intelligent and scalable framework for mix design optimization of green concrete incorporating recycled aggregates from precast rejects. Case Stud. Constr. Mater. 20, e03156.

Zhang, J.-P., Li, Z.-W., Yang, J., 2005. A parallel SVM training algorithm on large-scale classification problems. In: 2005 International Conference on Machine Learning and Cybernetics. IEEE.
Zhang, R., Ma, J., 2008. An improved SVM method P-SVM for classification of remotely sensed data. Int. J. Rem. Sens. 29 (20), 6029–6036.
Zhao, J., Yu, T., Teng, J., 2015. Stress-strain behavior of FRP-confined recycled aggregate concrete. J. Compos. Construct. 19 (3), 04014054.
Zhao, Q., et al., 2023. How can C&D waste recycling do a carbon emission contribution for construction industry in Japan city? Energy Build. 298, 113538.
Zhou, Y.-W., Wu, Y.-F., 2012. General model for constitutive relationships of concrete and its composite structures. Compos. Struct. 94 (2), 580–592.
Zhou, Y., et al., 2016. FRP-confined recycled coarse aggregate concrete: experimental investigation and model comparison. Polymers 8 (10), 375.
Zhu, L., Zhao, C., Dai, J., 2021. Prediction of compressive strength of recycled aggregate concrete based on gray correlation analysis. Constr. Build. Mater. 273, 121750.